Metal Atom Effect on the Photophysical Properties of Mg(II), Zn(II), Cd(II), and Pd(II) Tetraphenylporphyrin Complexes Proposed as Possible Drugs in Photodynamic Therapy

Bruna Clara De Simone, Gloria Mazzone [ID] **, Nino Russo *, Emilia Sicilia and Marirosa Toscano**

Dipartimento di Chimica e Tecnologie Chimiche, Università della Calabria, I-87036 Arcavacata di Rende, Italy; bruna.desimone@unical.it (B.C.D.S.); gloria.mazzone@unical.it (G.M.); siciliae@unical.it (E.S.); marirosa.toscano@unical.it (M.T.)
* Correspondence: nino.russo@unical.it; Tel.: +39-098-449-2106

Abstract: The effects of Mg, Zn, Cd, and Pd dications on the photophysical properties of the tetraphenylporphyrin ligand have been explored, considering the corresponding complexes and by using the density functional theory and its time-dependent extension. Results show that absorption wavelengths do not change significantly when the metal ion changes contrary to what happens to the singlet–triplet energy gaps (ΔE_{S-T}) and the spin-orbit matrix elements $\langle \Psi_{S_n} | \hat{H}_{so} | \Psi_{T_m} \rangle$. The most probable intersystem spin crossing (ISC) pathways for the population of the lowest triplet states have been explored. Our findings can contribute to rationalize the available experimental data and promote the potential therapeutic use of these compounds as photosensitizers in photodynamic therapy (PDT).

1. Introduction

The transitions between pure spin states of different multiplicities are, as it is well known, forbidden by the spin selection rules. However, several spin-forbidden intersystem crossings in organic and inorganic systems are reported to be essential for a specific action in different areas [1–3]. It is known that these transitions can occur as result of a spin–orbit coupling (SOC), a relativistic effect that induces a quantum mechanical mixing between states with different spin multiplicity. The SOC arises from the interaction between spin magnetic moment of an electron and the magnetic field resulting from the motion of the nucleus. Since the nuclear magnetic field depends on nuclear charge, the SOCs assume greater values with the increasing of the atomic number. High SOC values enhance the kinetics of both radiative and non-radiative transitions between states with different spin. Based on what has been said before, the intersystem crossing (ISC) is observed often in systems containing high atomic number elements. The phenomenon is, thus, known as heavy atom effect (HAE).

HAE plays an important role in determining many photophysical and photochemical properties. The phosphorescence lifetime of various substituted aromatic compounds has been associated with the spin–orbit coupling variation due to the presence of different heavy atoms in the examined species, for the first time by McClure's [4]. Later, the HAE in photophysics and photochemistry has assumed increasing importance [1,5,6]. Nowadays, a great deal of interest in the ISC process is related to design of novel materials useful in many fields such as photocatalytic organic and inorganic reactions, triplet-triplet annihilation, and photodynamic therapy (PDT).

PDT is a clinical therapeutic modality with great potential of application in various diseases, including cancer photo-treatment [7–13], but also in environmental and antimicrobial fields [14–17]. PDT combines the action of three key components: (i) the light, with specific wavelength; (ii) a photosensitizer; and (iii) molecular oxygen naturally present in the tissues, in order to produce reactive oxygen species, like singlet excited oxygen, as cytotoxic agents that are able to destroy diseased cells selectively. The success of this strategy lies in an effective ISC between singlet and triplet excited states of the employed photosensitizer. For this reason, the research on design and characterization of new drugs for PDT is a matter of great interest. An ideal PDT photosensitizer must possess, besides certain chemical properties, several photophysical properties. Among them, the most important are: (i) the absorption in the so-called photodynamic therapeutic window (500–900 nm) in order to maximize the penetration into the tissues; (ii) an efficient intersystem spin crossing to populate a triplet state ($S_n \rightarrow T_m$); (iii) a subsequent accessible triplet state energy transfer needed to excite the molecular oxygen from its $^3\Sigma_g$ ground state to the excited one $^1\Delta_g$. This means that the ΔE_{S-T} of the photosensitizer must be higher than 0.98 eV, the energy required to produce the cytotoxic agent ($^1O_2$) in type II photoreactions [18].

Several classes of compounds have been studied so far and the porphyrin-like systems (e.g., foscan, temocene, and their metal complexes) still remain one of the most interesting families [19–25]. The presence of a metal in the porphyrin-like cavity should, in principle, increase the ISC kinetics due the presence of a coordinated metal (internal heavy atom effect).

In this work, we have undertaken a systematic theoretical work, in the framework of Density Functional Theory (DFT) and its time-dependent extension (TDDFT), on the photophysical properties of Mg(II), Zn(II), Cd(II), and Pd(II) tetraphenylporphyrin (TPP) complexes (see Scheme 1). In particular, we have tried to elucidate the origin of the improved $^1\Delta_g$ production besides the excitation energies, the singlet-triplet energy gaps, the spin-orbit matrix elements, directly related to the intersystem crossing kinetics as postulated by the Fermi Golden Rule [26,27]. Moreover, different possible intersystem spin crossing pathways for the activation of the lowest triplet state have been explored and discussed on the basis of the obtained SOC and ΔE_{S-T} values taking into account the El-Sayed [28] and Kasha [29] rules.

M = Mg (MgTPP), Zn (ZnTPP),
Cd (CdTPP), Pd (PdTPP)
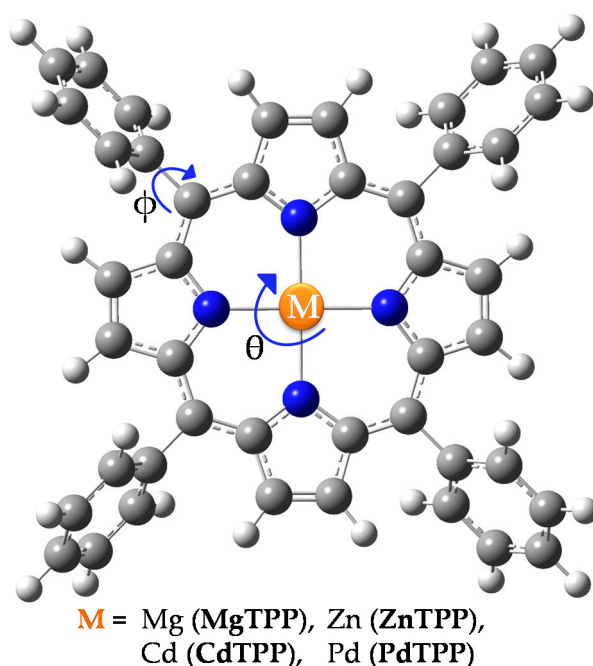
Scheme 1. Representation of the investigated metallotetraphenylporphyrines (MTPP, with M = Mg(II), Zn(II), Cd(II), Pd(II)).

2. Results and Discussion

Although optimizations have been carried out without imposing any constraints, resulting structures show D_{2d} geometries with a very slight deviation from planarity around the porphyrinoid core which occurs mainly for the triplets. The maximum deviation is found for the zinc complex in the T_2 excited state where θ has a value of 3.5°. The *meso* phenyl substituents lie out from the porphyrin ring plane in both ground and excited states of all the considered systems. The torsional angle (φ) is about 60° in the ground states and a variation of few degrees have been registered in the excited ones. Comparison with the experimental data is possible only for the zinc complex [30]. We find a Zn–N distance of 2.029 Å in good agreement with the X-ray counterpart [30] (2.037 Å). The agreement is also satisfactory with previous density functional studies in which different exchange-correlation functionals have been used [31,32]. As expected, in the excited states other geometrical parameters also change, but the variations are very small.

The computed excitation energies together with the available experimental data are collected in Table 1.

The analysis of the molecular orbitals energies has evidenced that HOMO and HOMO − 1, as well as LUMO and LUMO + 1, are doubly degenerate, in agreement with previous studies [31,32]. This means that the excited states generated by transitions involving degenerate orbitals result to be equally degenerate, such as S_1 and S'_1 deriving from H → L and H → L + 1 transitions (see Table 1), respectively. Therefore, only one value will be used for the discussion.

Table 1. Main vertical excitation energies (ΔE), absorption wavelengths (λ) Oscillator Strengths (*f*) and Transitions (Molecular Orbital contribution in %) for the studied compounds in benzene solvent, computed at the M06/6 − 31 + G * level of theory.

Compound	Excited State	λ_{theo} (nm)	ΔE (eV)	*f*	λ_{exp} (nm)	Transitions [d]
MgTPP	S_1 (S'_1)	559	2.22	0.008	607 [a]	H → L, 54% (H → L + 1, 54%)
	S_2 (S'_2)	404	3.07	1.739	428 [a]	H − 1 → L, 44% (H − 1 → L + 1, 44%)
	T_1 (T'_1)	831	1.49	0	794 [c]	H → L, 83% (H → L + 1, 83%)
	T_2 (T'_2)	630	1.97	0		H − 1→L, 84% (H − 1 → L + 1, 84%)
ZnTPP	S_1 (S'_1)	561	2.21	0.038	593 [a]	H → L, 50% (H → L + 1, 50%)
	S_2 (S'_2)	412	3.01	1.699	424 [a]	H − 1 → L + 1, 47% (H − 1 → L, 47%)
	T_1 (T'_1)	812	1.53	0	778 [c]	H → L, 70% (H → L + 1, 70%)
	T_2 (T'_2)	626	1.98	0		H − 1 → L, 82% (H − 1 → L + 1, 82%)
CdTPP	S_1 (S'_1)	549	2.26	0.013	617 [a]	H → L, 54% (H → L + 1, 54%)
	S_2 (S'_2)	397	3.12	1.670	437 [a]	H − 1 → L+1, 59% (H − 1 → L, 59%)
	T_1 (T'_1)	846	1.46	0	814 [c]	H → L, 52% (H → L + 1, 52%)
	T_2 (T'_2)	619	2.00	0		H − 1 → L, 85% (H – 1 → L + 1, 85%)
PdTPP	S_1 (S'_1)	537	2.31	0.032	553 [b]	H → L, 48% (H → L + 1, 48%)
	S_2 (S'_2)	409	3.03	1.519	407 [b]	H − 1 → L, 59% (H − 1 → L + 1, 59%)
	T_1 (T'_1)	758	1.63	0		H → L, 78% (H → L + 1, 78%)
	T_2 (T'_2)	597	2.07	0		H − 1 → L, 84% (H − 1 → L + 1, 84%)

[a] [33]; [b] [34] in CHCl$_3$; [c] [35]; [d] only the major contribution is reported.

As in the case of other porphyrin-like metal complexes [31], the D_{2d} molecular symmetry of metallotetraphenylporphyrin complexes MTPP is responsible of the single Q and Soret bands, generally split in two different bands in metal-free tetraphenylporphyrin. As usual, the Q band has a very low oscillator strength, while the Soret one is the most intense band. Both the singlet transitions are in satisfactory agreement with the experimental data [33–35], being the average error about 40 and 20 nm, respectively. The maximum deviation occurs for the Q band of **CdTPP** for which a difference from the experiment value of 68 nm has been found. The degenerate S_1 and S'_1 excited states, that fall in the Q region, are mainly originated by a H → L and H → L + 1 transitions, respectively, while the Soret band, with two degenerate states, is obtained by H − 1 → L (S_2) and H − 1 → L + 1 S'_2 transitions. The comparison of our results with the available experimental data concerning the lowest triplet excitation energies for Mg, Zn, and Cd-complexes [35] shows an excellent agreement (average error of

0.06 eV). On the basis of this evidence, we think that our prediction on the lowest triplet excitation energy for **PdTPP** complex should be reliable.

From the computed vertical transition energies that emerge in all the studied systems, the energy gap between the ground singlet and low lying triplet excited states ($\Delta E_{S_0-T_1}$) is higher than the energy required to excite the molecular oxygen in its $^1\Delta_g$ state (0.98 eV) and, consequently they are potential candidates to act as type II photosensitizers in PDT.

The production of cytotoxic singlet oxygen is directly related to the rate constant of the radiationless intersystem crossing (ISC) between S_n and T_m states. In the golden rule approximation [26,27], the ISC efficiency depends on the amplitude of the spin−orbit coupling and the related $\Delta E_{S_n-T_m}$ energy gaps. The first term is proportional to the squared module of the spin−orbit matrix element between the initial $\Psi(S_n)$ and final $\Psi(T_m)$ wave functions that depends on the nature of the orbitals involved in the transition (according to the El Sayed rules [28]). Heavy atoms can also affect the SOCs that increase as a function of Z^4 (heavy atom effect) being directly proportional to the atomic number and inversely proportional to the mean cubic radial distribution (r^{-3}) of the electron.

Given the presence of two low-lying singlet excited states and the existence of triplets below them, all the deactivation processes for the production of singlet oxygen depicted in Scheme 2 have been considered. In these paths, the deactivation can start from: (i) the first excited singlet state S_1 generated by a transition with very weak oscillator strength, or (ii) the second excited singlet state S_2 that can directly decay on the triplets or through a fast $S_2 \rightarrow S_1$ internal conversion. The available experimental data provide controversial interpretations about the origin of the emission for these systems [33–39]. In some studies, the emission band is interpreted as coming directly from S_2, whereas others suggest that the S_1 state is involved, assuming that an IC from S_2 to S_1 occurs. Although the first hypothesis, as mentioned above, is the most accredited we have considered the possible deactivation pathways taking into account both S_1 and S_2 excited states as the starting state for the population of the lowest triplet one. Therefore, in order to suggest the preferred deactivation path, the following SOCs have been computed: $\langle \Psi_{S_1}|\hat{H}_{so}|\Psi_{T_1}\rangle$, $\langle \Psi_{S_1}|\hat{H}_{so}|\Psi_{T_2}\rangle$, $\langle \Psi_{S_2}|\hat{H}_{so}|\Psi_{T_1}\rangle$ and $\langle \Psi_{S_2}|\hat{H}_{so}|\Psi_{T_2}\rangle$. Table 2 reports these values together with the relative $\Delta E_{S_n-T_m}$ values.
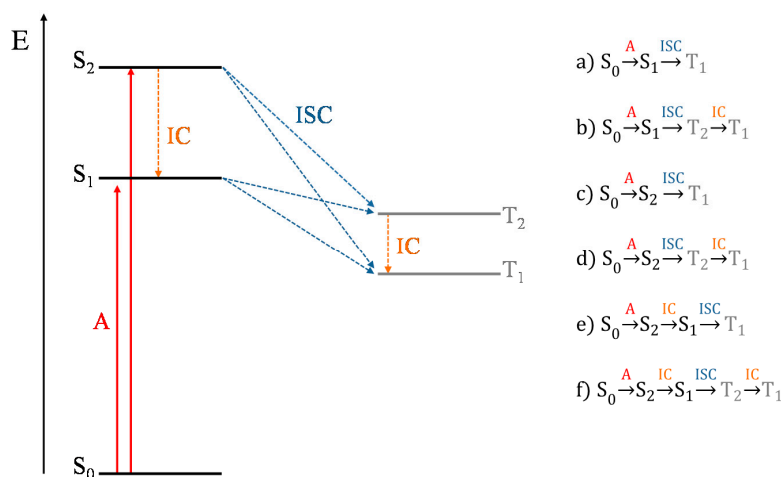
Scheme 2. Representative energy diagram of the excited singlet and triplet states and likely deactivation pathways (**a–f**).

In the first pathway (a), the T_1 state can be populated by a direct ISC from S_1 state while in the second (b) the $S_1 \rightarrow T_2$ ISC is followed by a fast IC to the lowest triplet state T_1. For all the MTPP systems the $\langle \Psi_{S_1}|\hat{H}_{so}|\Psi_{T_1}\rangle$ term assumes the greatest value and the energy gap between the involved excited states, $\Delta E_{S_1-T_1}$, is about 0.7 eV. The decay of S_2 to triplets T_1 and T_2 is taken into account in paths (**c**) and (**d**), respectively. From the computed SOCs and singlet–triplet energy gaps (see Table 2) it seems that the path (**d**), involving $S_2 \rightarrow T_2$ radiationless transition, is the preferred one.

However, the SOC values end up being smaller than those found for the ISC involving the S_1 state. In the hypothesized deactivation (**e**) and (**f**) channels, a primary IC from S_2 to S_1 is followed by the ISC to the T_1 or T_2 states, respectively. As just mentioned, the obtained $\langle \Psi_{S_1}|\hat{H}_{so}|\Psi_{T_1}\rangle$ values, being approximately twice than those computed for the $S_1 \rightarrow T_2$ transition, suggest the pathway (**e**) as the most probable one. This is in agreement with the El Sayed [28] and Kasha [29] rules.

From Table 2, it clearly appears how the nature of the central metal ion affects the spin–orbit coupling amplitude. As expected, the largest SOC values are obtained for **PdTPP**. The radiationless process involves excited states that are mainly π–π^* in nature, with a modest participation of d metal orbitals that becomes consistent in the T_1 and T_2 states (see Figure 1).

In order to compare our results with the available experimental ones, we have reported, in Figure 2, the trend of both the experimentally determined triplet quantum yields (φ_T) [35] and our SOC values. As shown in figure, the increase of φ_T as a function of metal atom size is well reproduced by the trend of $\langle \Psi_{S_1}\hat{H}_{so}|\Psi_{T_1}\rangle$ along the series, especially in the cases of **MgTPP** and **PdTPP**.

Although deactivation pathways that involve the ISC between S_1 and T_1 seem to be the main events, other paths can contribute to the production of singlet oxygen since all the computed SOCs are higher than that computed for Foscan® (2.4×10^{-1} cm^{-1} for the $S_1 \rightarrow T_1$ transition) [22], the photosensitizer already used in photodynamic therapy.

Table 2. SOC values (cm^{-1}) and energy gaps ($\Delta E_{S_n - T_m}$ eV) between the involved excited states calculated at B3LYP/cc-pVDZ//M06/6 − 31G * and M06/6 − 31 + G* levels of theory.

	MgTPP	ZnTPP	CdTPP	PdTPP
$\|\langle \Psi_{S_1}\|\hat{H}_{so}\|\Psi_{T_1}\rangle\|$	0.31	1.64	14.01	28.99
$\Delta E_{S_1-T_1}$	0.73	0.68	0.80	0.68
$\|\langle \Psi_{S_1}\|\hat{H}_{so}\|\Psi_{T_2}\rangle\|$	0.15	0.70	9.55	12.81
$\Delta E_{S_1-T_2}$	0.25	0.23	0.26	0.24
$\|\langle \Psi_{S_2}\|\hat{H}_{so}\|\Psi_{T_1}\rangle\|$	0.14	0.38	0.52	4.10
$\Delta E_{S_2-T_1}$	1.58	1.48	1.66	1.40
$\|\langle \Psi_{S_2}\|\hat{H}_{so}\|\Psi_{T_2}\rangle\|$	0.22	0.05	4.52	16.97
$\Delta E_{S_2-T_2}$	1.10	1.03	1.12	0.96
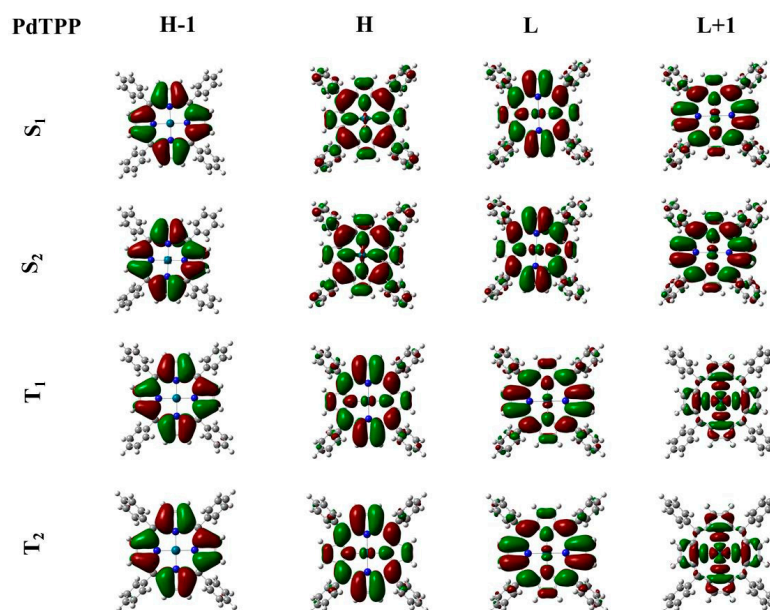
Figure 1. Graphical representation of the HOMO − 1, HOMO, LUMO and LUMO + 1 for S_1, S_2, T_1, T_2 states of **PdTPP** computed at M06/6 − 31G * level of theory.
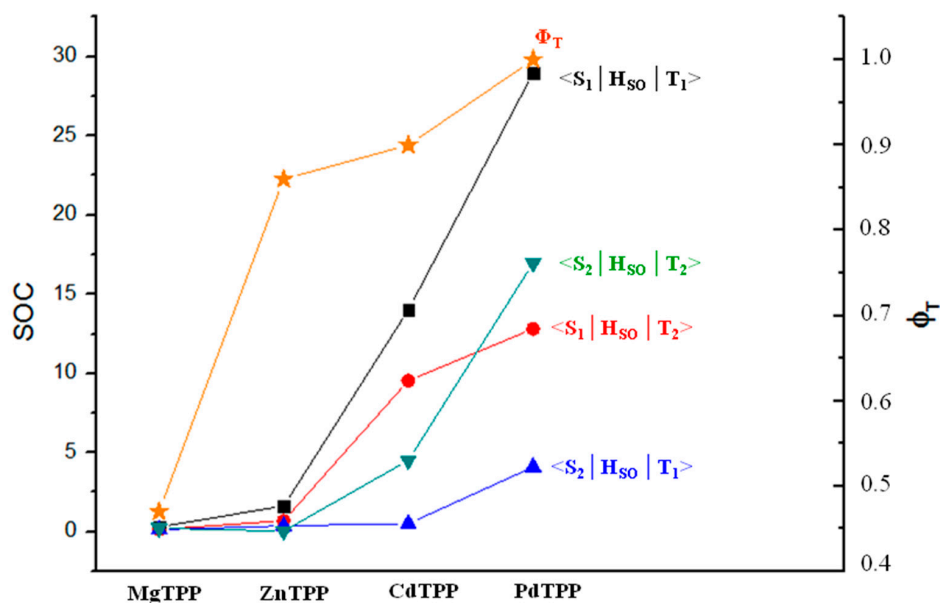
Figure 2. Computed SOCs (cm^{-1}) for S$_n$–T$_m$ (with n and m = 1, 2) radiationless transitions and measured [35] triplet quantum yields φ_T for the investigated systems.

3. Computational Methods

Ground and excited state optimizations have been performed by using M06 [40] exchange correlation functional coupled with the all electron 6-31G* basis sets for all the atoms except for Cd and Pd, for which the SSD pseudopotential has been employed for DFT and TDDFT levels of theory. DFT and TDDFT approaches have been successfully applied to study the photophysical properties of similar and other systems [22–25,41–47].

The excitation energies have been calculated by substituting the $6 - 31G*$ basis set with the $6 - 31 + G*$ one. Solvent effects have been included in the excitation energy computations by means of integral equation formalism polarizable continuum model (IEFPCM) [48,49]. Since the experimental data [33–35] have been obtained in benzene solution, we have considered this solvent (ε = 2.27). All these computations have been carried out by using Gaussian 09 code [50].

SOC elements have been computed with DALTON code [51] by using the spin–orbit coupling operators for effective core potentials with the effective nuclear charge [52] for systems containing Cd and Pd atoms, while atomic-mean field approximation [53] is used in the other cases. Due to the limited number of functionals implemented in this code for quadratic response calculations, the B3LYP [54,55] has been employed. The cc-pVDZ basis set has been used for all the atoms with the exception of Cd and Pd, which we have described using the cc-pVDZ-PP one.

The spin–orbit couplings (SOCs) have been defined according to the following formula

$$\mathrm{SOC}_{ij} = \sqrt{\sum_n \left| \left\langle \psi_{S_i} | \hat{H}_{SO} | \psi_{T_{j,n}} \right\rangle \right|^2}; \ n = x, y, z \tag{1}$$

where $\hat{H}_{SO}$ is the spin–orbit Hamiltonian.

4. Conclusions

Metal atom effect on the photophysical properties of metals containing tetraphenylporphyrin has been determined by using DFT and TDDFT theoretical based methods. Our results show that the employed computational protocol, that is M06/$6 - 31 + G*$, is able to reasonably reproduce the experimental absorption wavelengths with errors of a few tens of nm. Our computations have

confirmed that the Q band lies over 550 nm, falling in the low region of the so-called therapeutic window. The evaluation of the low-lying triplet states has evidenced the possibility of all considered MTPP to be able to generate the cytotoxic agent in type II PDT photoreactions, as ΔE_{S-T} gaps are greater than the energy required to excite the molecular oxygen (experimental value 0.98 eV).

Moreover, the introduction of the metal ion in the cavity of porphyrin-like moiety and its nature induce an increase of the spin−orbit matrix elements proportionally with the increase of the atomic number. Following the El Sayed rules, the most efficient intersystem crossing occurs for **PdTPP** in which the transition between two states with different spin multiplicities involves orbitals with different shapes.

Even if all the investigated systems own photophysical properties that make them suitable to be used as photosensitizers in photodynamic therapy, we suggest the magnesium and palladium containing compounds as the best PS candidates in PDT. We hope that our investigation can stimulate further experimental work on these promising photosensitizers.

Author Contributions: Bruna Clara De Simone, Gloria Mazzone, Nino Russo, Emilia Sicilia, and Marirosa Toscano made equal contributions to the study and the publication of this work.

Conflicts of Interest: The authors declare no conflict of interest.

References

1. Marian, C.M. Spin-orbit coupling and intersystem crossing in molecules. *Wiley Interdiscip. Rev. Comput. Mol. Sci.* **2012**, *2*, 187–203. [CrossRef]

2. Fantacci, S.; De Angelis, F. Impact of Spin-Orbit Coupling on Photocurrent Generation in Ruthenium Dye-Sensitized Solar Cells. *J. Phys. Chem. Lett.* **2014**, *5*, 375–380. [CrossRef] [PubMed]

3. Kannan, U.M.; Muddisetti, V.N.; Kotnana, G.; Kandhadi, J.; Giribabu, L.; Singh, S.P.; Jammalamadaka, S.N. Spin–orbit coupling and Lorentz force enhanced efficiency of TiO_2-based dye sensitized solar cells. *Phys. Status Solidi A* **2017**, *214*, 1600691. [CrossRef]

4. McClure, D.S. Spin-Orbit Interaction in Aromatic Molecules. *J. Chem. Phys.* **1952**, *20*, 682–688. [CrossRef]

5. De Simone, B.C.; Mazzone, G.; Pirillo, J.; Russo, N.; Sicilia, E. Halogen atom effect on the photophysical properties of substituted aza-BODIPY derivatives. *Phys. Chem. Chem. Phys.* **2017**, *19*, 2530–2536. [CrossRef] [PubMed]

6. Alberto, M.E.; De Simone, B.C.; Mazzone, G.; Sicilia, E.; Russo, N. The Heavy Atom Effect on Zn(II) Phthalocyanine Derivatives: A Theoretical Exploration of the Photophysical Properties. *Phys. Chem. Chem. Phys.* **2015**, *17*, 23595–23601. [CrossRef]

7. Awuah, S.G.; You, Y. Boron dipyrromethene (BODIPY)-based photosensitizers for photodynamic therapy. *RSC Adv.* **2012**, *2*, 11169–11183. [CrossRef]

8. Dougherty, T.J.; Grindey, G.B.; Fiel, R.; Weishaupt, K.R.; Boyle, D.G.J. Photoradiation therapy. II. Cure of animal tumors with hematoporphyrin and light. *J. Natl. Cancer Inst.* **1975**, *55*, 115–121. [CrossRef] [PubMed]

9. Juzeniene, A.; Peng, Q.; Moan, J. Milestones in the development of photodynamic therapy and fluorescence diagnosis. *Photochem. Photobiol. Sci.* **2007**, *6*, 1234–1245. [CrossRef]

10. Babilas, P.; Schreml, S.; Landthaler, M.; Szeimies, R.M. Photodynamic therapy in dermatology: State-of-the-art. *Photodermatol. Photoimmunol. Photomed.* **2010**, *26*, 118–132. [CrossRef] [PubMed]

11. Kossodo, S.; La Muraglia, G.M. Clinical potential of photodynamic therapy in cardiovascular disorders. *Am. J. Cardiovasc. Drugs* **2001**, *1*, 15–21. [CrossRef] [PubMed]

12. Garrier, J.; Bezdetnaya, L.; Barlier, C.; Gräfe, S.; Guillemin, F.; D'Hallewin, M.A. Foslip®-based photodynamic therapy as a means to improve wound healing. *Photodiagn. Photodyn. Ther.* **2011**, *8*, 321–327. [CrossRef] [PubMed]

13. Dąbrowski, J.M.; Arnaut, L.G. Photodynamic therapy (PDT) of cancer: From local to systemic treatment. *Photochem. Photobiol. Sci.* **2015**, *14*, 1765–1780. [CrossRef] [PubMed]

14. Kim, H.; Kim, W.; Mackeyev, Y.; Lee, G.-S.; Kim, H.-J.; Tachikawa, T.; Hong, S.; Lee, S.; Kim, J.; Wilson, L.J.; Majima, T.; Alvarez, P.J.J.; Choi, W.; Lee, J. Selective Oxidative Degradation of Organic Pollutants by Singlet Oxygen-Mediated Photosensitization: Tin Porphyrin versus C_{60} Aminofullerene Systems. *Environ. Sci. Technol.* **2012**, *46*, 9606–9613. [CrossRef] [PubMed]

15. Han, S.K.; Sik, R.H.; Motten, A.G.; Chignell, C.F.; Bilski, P.J. Photosensitized oxidation of tetrabromobisphenol a by humic acid in aqueous solution. *Photochem. Photobiol.* **2009**, *85*, 1299–1305. [CrossRef] [PubMed]

16. Kohn, T.; Nelson, K.L. Sunlight-mediated inactivation of MS2 coliphage via exogenous singlet oxygen produced by sensitizers in natural waters. *Environ. Sci. Technol.* **2007**, *41*, 192–197. [CrossRef] [PubMed]

17. Romero, O.C.; Straub, A.P.; Kohn, T.; Nguyen, T.H. Role of temperature and Suwannee River natural organic matter on inactivation kinetics of rotavirus and bacteriophage MS2 by solar irradiation. *Environ. Sci. Technol.* **2011**, *45*, 10385–10393. [CrossRef] [PubMed]

18. Plaetzer, K.; Krammer, B.; Berlanda, J.; Berr, F.; Kiesslich, T. Photophysics and photochemistry of photodynamic therapy: fundamental aspects. *Lasers Med. Sci.* **2009**, *24*, 259–268. [CrossRef] [PubMed]

19. Ethirajan, M.; Chen, Y.; Joshi, P.; Pandey, R.K. The role of porphyrin chemistry in tumor imaging and photodynamic therapy. *Chem. Soc. Rev.* **2013**, *42*, 845–856. [CrossRef] [PubMed]

20. Banfi, S.; Caruso, E.; Caprioli, S.; Mazzagatti, L.; Canti, G.; Ravizza, R.; Gariboldi, M.; Monti, E. Photodynamic effects of porphyrin and chlorin photosensitizers in human colon adenocarcinoma cells. *Bioorg. Med. Chem.* **2004**, *12*, 4853–4860. [CrossRef] [PubMed]

21. Garcıa-Dıaz, M.; Sanchez-Garcıa, D.; Soriano, J.; Sagrist, M.L.; Mora, M.; Villanueva, A.; Stockert, J.C.; Canete, M.; Nonell, S. Temocene: The porphycene analogue of temoporfin (Foscan®). *MedChemComm* **2011**, *2*, 616–619. [CrossRef]

22. Alberto, M.E.; Marino, T.; Quartarolo, A.D.; Russo, N. Photophysical origin of the reduced photodynamic therapy activity of temocene compared to Foscan®: Insights from theory. *Phys. Chem. Chem. Phys.* **2013**, *15*, 16167–16171. [CrossRef] [PubMed]

23. Alberto, M.E.; De Simone, B.C.; Mazzone, G.; Marino, T.; Russo, N. Photophysical properties of free and metallated meso-substituted tetrabenzotriazaporphyrin from density functional theory investigation. *Dyes Pigm.* **2015**, *120*, 335–339. [CrossRef]

24. Mazzone, G.; Alberto, M.E.; De Simone, B.C.; Marino, T.; Russo, N. Can Expanded Bacteriochlorins Act as Photosensitizers in Photodynamic Therapy? Good News from Density Functional Theory Computations. *Molecules* **2016**, *21*, 288. [CrossRef] [PubMed]

25. Mazzone, G.; Russo, N.; Sicilia, E. Theoretical investigation of the absorption spectra and singlet-triplet energy gap of positively charged tetraphenylporphyrins as potential photodynamic therapy photosensitizers. *Can. J. Chem.* **2013**, *91*, 902–906. [CrossRef]

26. Lawetz, V.; Orlandi, G.; Siebrand, J.W. Theory of Intersystem Crossing in Aromatic Hydrocarbons. *J. Chem. Phys.* **1972**, *56*, 4058–4072. [CrossRef]

27. Robinson, G.W.; Frosch, R.P.J. Electronic Excitation Transfer and Relaxation. *J. Chem. Phys.* **1963**, *38*, 1187–1203. [CrossRef]

28. El-Sayed, M.A. Triplet state. Its radiative and nonradiative properties. *Acc. Chem. Res.* **1968**, *1*, 8–16. [CrossRef]

29. Kasha, M. Characterization of Electronic Transitions in Complex Molecules. *Discuss. Faraday Soc.* **1950**, *9*, 14–19. [CrossRef]

30. Scheidt, W.R.; Mondal, J.U.; Eigenbrodt, C.W.; Adler, A.; Radonvich, L.J.; Hoard, J.L. Crystal and Molecular Structure of the Silver(II) and Zinc(II) Derivatives of meso-Tetraphenylporphyrin. An Exploration of Crystal-Packing Effects on Bond Distance. *Inorg. Chem.* **1986**, *25*, 795–799. [CrossRef]

31. Nguyen, K.A.; Day, P.N.; Pachter, R.; Tretiak, S.; Chernyak, V.; Mukamel, S. Analysis of Absorption Spectra of Zinc Porphyrin, Zinc meso-Tetraphenylporphyrin, and Halogenated Derivatives. *J. Phys. Chem. A* **2002**, *106*, 10285–10293. [CrossRef]

32. Liu, X.; Yeow, E.K.L.; Velate, S.; Steer, R.P. Photophysics and spectroscopy of the higher electronic states of zinc metalloporphyrins: A theoretical and experimental study. *Phys. Chem. Chem. Phys.* **2006**, *8*, 1298–1309. [CrossRef] [PubMed]

33. Tripathy, U.; Kowalska, D.; Liu, X.; Velate, S.; Steer, R.P. Photophysics of Soret-Excited Tetrapyrroles in Solution. I. Metalloporphyrins: MgTPP, ZnTPP, and CdTPP. *J. Phys. Chem. A* **2008**, *112*, 5824–5833. [CrossRef] [PubMed]

34. Obata, M.; Hirohara, S.; Tanaka, R.; Kinoshita, I.; Ohkubo, K.; Fukuzumi, S.; Tanihara, M.; Yano, S. In Vitro Heavy-Atom Effect of Palladium(II) and Platinum(II) Complexes of Pyrrolidine-Fused Chlorin in Photodynamic Therapy. *J. Med. Chem.* **2009**, *52*, 2747–2753. [CrossRef] [PubMed]

35. Azenha, E.G.; Serra, A.C.; Pineiro, M.; Pereira, M.M.; Seixas de Melo, J.; Arnauta, L.G.; Formosinho, S.J.; Rocha Gonsalves, A.M.d'A. Heavy-atom effects on metalloporphyrins and polyhalogenated porphyrins. *Chem. Phys.* **2002**, *280*, 177–190. [CrossRef]

36. Yu, H.Z.; Baskin, J.S.; Zewail, A.H. Ultrafast Dynamics of Porphyrins in the Condensed Phase: II. Zinc Tetraphenylporphyrin. *J. Phys. Chem. A* **2002**, *106*, 9845–9854. [CrossRef]

37. Ghosh, M.; Mora, A.K.; Nath, S.; Chandra, A.K.; Hajra, A.; Sinha, S. Photophysics of Soret-excited free base tetraphenylporphyrin and its zinc analog in solution. *Spectrochim. Acta Part A Mol. Biomol. Spectrosc.* **2013**, *116*, 466–472. [CrossRef] [PubMed]

38. Pineiro, M.; Carvalho, A.L.; Pereira, M.M.; Rocha Gonsalves, A.M.d'A.; Arnaut, L.G.; Formosinho, S.J. Photoacoustic Measurements of Porphyrin Triplet-State Quantum Yields and Singlet-Oxygen Efficiencies. *Chem. Eur. J.* **1998**, *4*, 2299–2307. [CrossRef]

39. Dabrowski, J.M.; Pucelik, B.; Regiel-Futyra, A.; Brindell, M.; Mazuryk, O.; Kyzioł, A.; Stochel, G.; Macyk, W.; Arnaut, L.G. Engineering of relevant photodynamic processes through structural modifications of metallotetrapyrrolic photosensitizers. *Coordinat. Chem. Rev.* **2016**, *325*, 67–101. [CrossRef]

40. Zhao, Y.; Truhlar, D.G. The M06 Suite of Density Functionals for Main Group Thermochemistry, Thermochemical Kinetics, Noncovalent Interactions, Excited States, and Transition Elements: Two New Functionals and Systematic Testing of Four M06-Class Functionals and 12 Other Functionals. *Theor. Chem. Acc.* **2008**, *120*, 215–241.

41. Pirillo, J.; De Simone, B.C.; Russo, N. Photophysical Properties Prediction of Selenium- and Tellurium-Substituted Thymidine as Potential UVA Chemotherapeutic Agents. *Theor. Chem. Acc.* **2016**, *135*, 8. [CrossRef]

42. Pirillo, J.; Mazzone, G.; Russo, N.; Bertini, L. Photophysical Properties of S, Se and Te-Substituted Deoxyguanosines: Insight into Their Ability to Act as Chemotherapeutic Agents. *J. Chem. Inf. Model.* **2017**, *57*, 234–242. [CrossRef] [PubMed]

43. Mazzone, G.; Quartarolo, A.D.; Russo, N. PDT-Correlated Photophysical Properties of Thienopyrrole BODIPY Derivatives. Theoretical Insights. *Dyes Pigm.* **2016**, *130*, 9–15. [CrossRef]

44. Alberto, M.E.; Mazzone, G.; Quartarolo, A.D.; Sousa, F.F.R.; Sicilia, E.; Russo, N. Electronic Spectra and Intersystem Spin-Orbit Coupling in 1,2- and 1,3-Squaraines. *J. Comput. Chem.* **2014**, *35*, 2107–2113. [CrossRef] [PubMed]

45. Jacquemin, D.; Perpète, E.A.; Ciofini, I.; Adamo, C. Accurate Simulation of Optical Properties in Dyes. *Acc. Chem. Res.* **2009**, *42*, 326–334. [CrossRef] [PubMed]

46. Eriksson, E.S.E.; Eriksson, L.A. Predictive Power of Long- Range Corrected Functionals on the Spectroscopic Properties of Tetrapyrrole Derivatives for Photodynamic Therapy. *Phys. Chem. Chem. Phys.* **2011**, *13*, 7207–7217. [CrossRef] [PubMed]

47. Adamo, C.; Jacquemin, D. The Calculations of Excited-State Properties with Time-Dependent Density Functional Theory. *Chem. Soc. Rev.* **2013**, *42*, 845–856. [CrossRef] [PubMed]

48. Cossi, M.; Barone, V. Solvent Effect on Vertical Electronic Transitions by the Polarizable Continuum Model. *J. Chem. Phys.* **2000**, *112*, 2427–2435. [CrossRef]

49. Tomasi, J.; Menucci, B.; Cammi, R. Quantum Mechanical Continuum Solvation Models. *Chem. Rev.* **2005**, *105*, 2999–3094. [CrossRef] [PubMed]

50. Frisch, M.J.; Trucks, G.W.; Schlegel, H.B.; Scuseria, G.E.; Robb, M.A.; Cheeseman, J.R.; Scalmani, G.; Barone, V.; Mennucci, B.; Petersson, G.A.; et al. *Gaussian 09*; Revision D.01; Gaussian, Inc.: Wallingford, CT, USA, 2009.

51. Aidas, K.; Angeli, C.; Bak, K.L.; Bakken, V.; Bast, R.; Boman, L.; Christiansen, O.; Cimiraglia, R.; Coriani, S.; Dahle, P.; et al. The Dalton quantum chemistry program system. *WIREs Comput. Mol. Sci.* **2014**, *4*, 269–284. [CrossRef] [PubMed]

52. Koseki, S.; Schmidt, M.W.; Gordon, M.S. Effective Nuclear Charges for the First- Through Third-Row Transition Metal Elements in Spin-Orbit Calculations. *J. Phys. Chem. A* **1998**, *102*, 10430–10436.

53. Ruud, K.; Schimmelpfennig, B.; Ågren, H. Internal and external heavy-atom effects on phosphorescence radiative lifetimes calculated using a mean-field spin-orbit Hamiltonian. *Chem. Phys. Lett.* **1999**, *310*, 215–221. [CrossRef]

54. Becke, A.D. Density-Functional Thermochemistry. III. The Role of Exact Exchange. *J. Chem. Phys.* **1993**, *98*, 5648–5652. [CrossRef]

55. Lee, C.; Yang, W.; Parr, R.G. Development of the Colle-Salvetti Correlation-Energy Formula into a Functional of the Electron Density. *Phys. Rev. B: Condens. Matter Mater. Phys.* **1988**, *37*, 785–789. [CrossRef]